GEOLOGY | THE GEOLOGICAL SOCIETY OF AMERICA®

https://doi.org/10.1130/G48069.1

Manuscript received 26 June 2020
Revised manuscript received 18 September 2020
Manuscript accepted 25 September 2020

Published online 10 December 2020

A novel authigenic magnetite source for sedimentary magnetization

Zhiyong Lin[1,2,3*], Xiaoming Sun[1,3,4,5*], Andrew P. Roberts[6], Harald Strauss[2], Yang Lu[7], Xin Yang[1], Junli Gong[1], Guanhua Li[4], Benjamin Brunner[8] and Jörn Peckmann[7]

[1]School of Marine Sciences, Sun Yat-sen University, Guangzhou 510006, China
[2]Institut für Geologie und Paläontologie, Westfälische Wilhelms-Universität Münster, Münster D-48149, Germany
[3]Guangdong Provincial Key Laboratory of Marine Resources and Coastal Engineering, Guangzhou 510006, China
[4]School of Earth Science and Engineering, Sun Yat-sen University, Guangzhou 510275, China
[5]Southern Laboratory of Ocean Science and Engineering (Guangdong, Zhuhai), Zhuhai 519000, China
[6]Research School of Earth Sciences, Australian National University, Canberra, Australian Capital Territory 2601, Australia
[7]Institut für Geologie, Zentrum für Erdsystemforschung und Nachhaltigkeit, Universität Hamburg, Hamburg D-20146, Germany
[8]Department of Geological Sciences, The University of Texas at El Paso, El Paso, Texas 79902, USA

ABSTRACT

We report a novel authigenic nanoscale magnetite source in marine methane seep sediments. The magnetite occurs in large concentrations in multiple horizons in a 230 m sediment core with gas hydrate–bearing intervals. In contrast to typical biogenic magnetite produced by magnetotactic bacteria and dissimilatory iron-reducing bacteria, most particles have sizes of 200–800 nm and many are aligned in distinctive structures that resemble microbial precipitates. The magnetite is interpreted to be a byproduct of microbial iron reduction within methanic sediments with rapidly changing redox conditions. Iron sulfides that accumulated at a shallow sulfate-methane transition zone were oxidized after methane seepage intensity decreased. The alteration process produced secondary iron (oxyhydr)oxides that then became a reactive iron source for magnetite authigenesis when methane seepage increased again. This interpretation is consistent with ^{13}C depletion in coexisting carbonate nodules. The authigenic magnetite will record younger paleomagnetic signals than surrounding sediments, which is important for paleomagnetic interpretations in seep systems. The microbial and possibly abiotic processes that caused these magnetic minerals to form at moderate burial depths remain to be determined.

INTRODUCTION

Magnetic signals preserved in sediments provide fundamental information for ancient tectonic, geomagnetic field, and environmental reconstructions. Sedimentary magnetic signals have traditionally been thought to be dominated by detrital magnetic iron-oxide particles, while biogenic magnetite with magnetically ideal stable single-domain (SD) properties has proven more recently to be a significant recorder of strong and stable sedimentary remanences over geological time scales (Chang and Kirschvink, 1989; Kopp and Kirschvink, 2008; Roberts et al., 2012). There are two main pathways for biomineralization of ultrafine biogenic magnetite in sediments, one of which is used by magnetotactic bacteria (MTB) and the other by dissimilatory iron-reducing bacteria (DIRB) (Moskowitz, 1995; Roberts, 2015). Intracellular magnetite produced by MTB has well defined sizes, morphologies, chain arrangements, and stoichiometries (Devouard et al., 1998; Kopp and Kirschvink, 2008). The magnetic nanoparticulate remains of MTB are preserved post-mortem as magnetofossils and are found in diverse sedimentary environments (Chang and Kirschvink, 1989). In contrast, extracellular authigenic magnetite produced by DIRB (Lovley et al., 1987) is thought to have sizes <20 nm in diameter (Li et al., 2009) with magnetically unstable superparamagnetic properties (Moskowitz et al., 1993). Although dissimilatory iron reducers occur widely in anoxic subsurface sediments, geological preservation of extracellular magnetite has been documented only rarely (e.g., Roberts, 2015).

Sulfidic diagenetic environments occur commonly within continental margin sediments with high organic matter or methane fluxes (Jørgensen, 1982; Boetius et al., 2000). Sulfidic conditions cause magnetite dissolution, which limits its geological preservation (Riedinger et al., 2005; Roberts, 2015). Typically, surface magnetizations are depleted rapidly at the sulfate-methane transition zone (SMTZ) where hydrogen sulfide is released by sulfate-driven anaerobic oxidation of methane (Boetius et al., 2000; Jørgensen et al., 2004), which promotes magnetite dissolution (Riedinger et al., 2005; Roberts, 2015). In contrast, we document here abnormally high magnetic susceptibilities at multiple inferred SMTZs from a methane seep site that are due to abundant, well-preserved magnetite nanoparticles. Magnetic, mineralogical, and geochemical analyses are presented to reveal the nature of these particles.

MAGNETIC SIGNALS RECORDED IN METHANIC SEDIMENTS

The study site GMGS2-16 is situated on the passive continental margin of the northern South China Sea (Fig. 1), which contains large basins with thick sedimentary sequences that have been deformed by movement along tectonic lineaments (McDonnell et al., 2000). Abundant methane-derived carbonates and gas hydrates (Fig. 1) confirm that methane seepage occurs widely in the study area (see the Supplemental Material[1] for materials and methods).

Mass magnetic susceptibility (χ) of sediments in core GMGS2-16 has large variations

*E-mails: linzhiy9@mail.sysu.edu.cn; eessxm@mail.sysu.edu.cn

[1]Supplemental Material. Geological background, methods, and further morphologies of iron (oxyhydr)oxides and FORC diagrams (Figures S1–S3). Please visit https://doi.org/10.1130/GEOL.S.13150895 to access the supplemental material, and contact editing@geosociety.org with any questions.

CITATION: Lin, Z., et al., 2021, A novel authigenic magnetite source for sedimentary magnetization: Geology, v. 49, p. 360–365, https://doi.org/10.1130/G48069.1

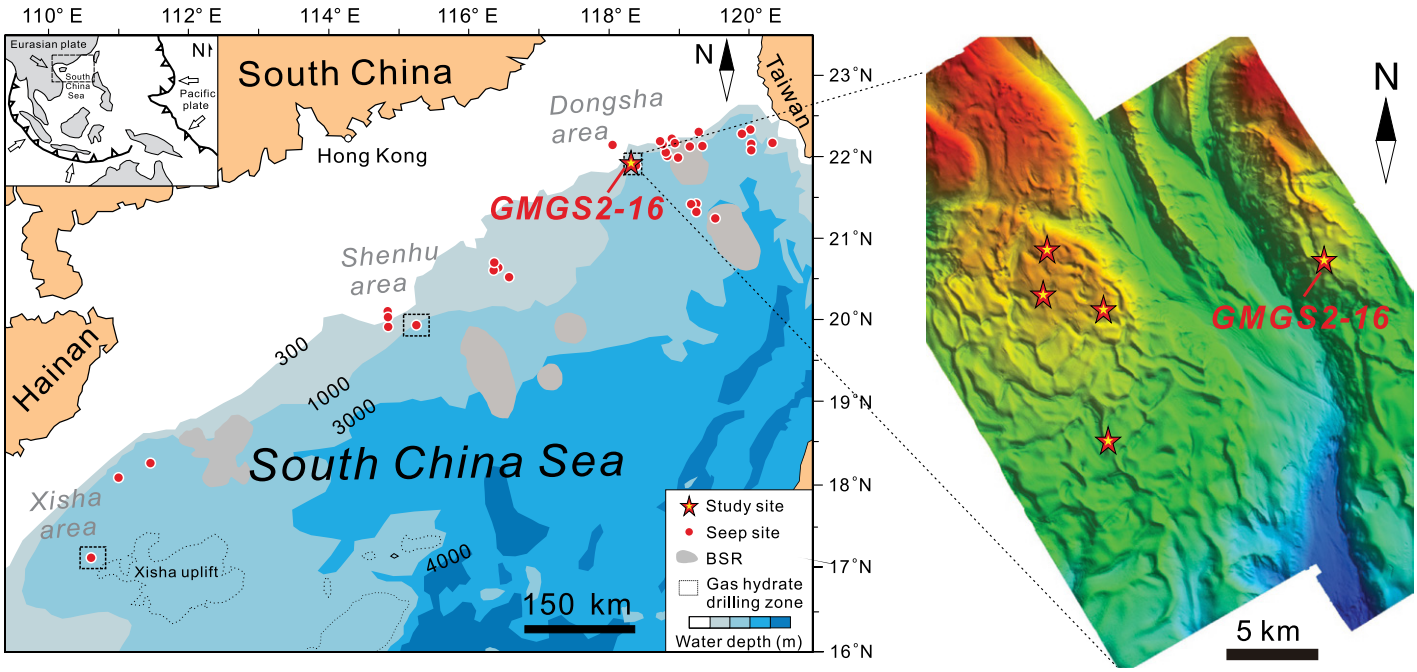

Figure 1. Location of study site GMGS2-16 in the South China Sea (left), and a seafloor bathymetric map of the locations of five gas hydrate-bearing cores (right) (after Sha et al., 2015). BSR—bottom simulating reflector.

(Fig. 2A). Peak χ values (>2 × 10^{-4} m^3 kg^{-1}) occur in multiple layers with nodular magnetic mineral aggregates (Figs. 3A and 3B; Fig. S1 in the Supplemental Material). In contrast, χ has low and constant values of ~1.0 × 10^{-4} m^3 kg^{-1} in intervals without magnetic aggregates. To characterize the magnetic domain state and magnetostatic interactions of magnetic particles, first-order reversal curve (FORC) measurements (Pike et al., 1999) were produced for bulk sediments. FORC diagrams for low-χ samples reveal a low-coercivity component and a magnetostatically interacting higher-coercivity SD component (Fig. 2E1; Figs. S2A–S2C); the latter is typical of greigite-bearing sediments that have experienced

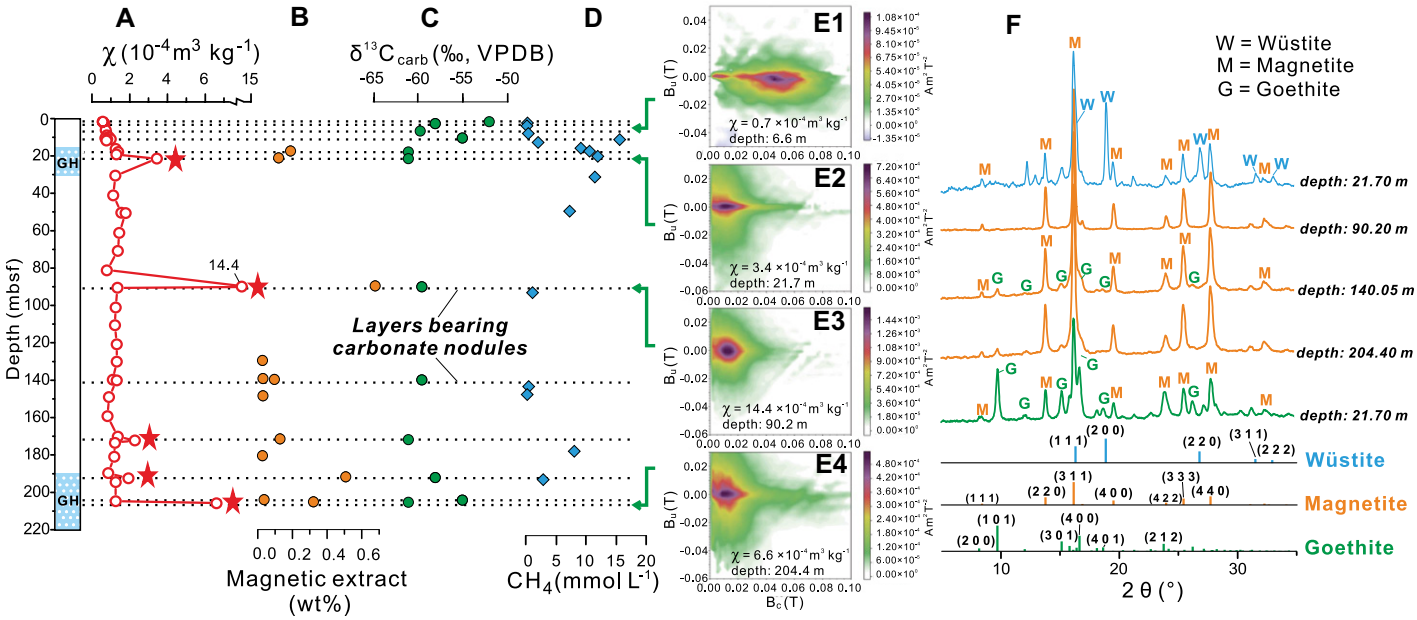

Figure 2. Magnetic, geochemical, and mineralogical data for core GMGS2-16 in the South China Sea (mbsf—meters below seafloor; GH—gas hydrate). (A) Magnetic susceptibility (χ) of bulk samples. (B) Magnetic extract as a percentage of bulk sediment. (C) Carbonate nodules and their $\delta^{13}C$ values (VPDB—Vienna Peedee belemnite). (D) Sedimentary methane concentrations (Sha et al., 2019). (E) First-order reversal curve (FORC) diagrams for bulk samples. FORC diagrams were processed using the FORCsensei algorithm (Heslop et al., 2020), which was used to search 1350 FORC models using all combinations of VARIFORC smoothing parameters (Egli, 2013) to produce optimal FORC distributions in which noise is smoothed without over-smoothing the underlying signal (https://forcaist.github.io/FORCaist.github.io/). Optimal VARIFORC parameters for each diagram in this figure are (1) $s_{c,0}$ = 4, $s_{c,1}$ = 4, $s_{u,0}$ = 2, $s_{u,1}$ = 3, λ = 0.08, and ψ = 0.25; (2) $s_{c,0}$ = 3, $s_{c,1}$ = 3, $s_{u,0}$ = 2, $s_{u,1}$ = 3, λ = 0.08, and ψ = 0.71; (3) $s_{c,0}$ = 2, $s_{c,1}$ = 2, $s_{u,0}$ = 2, $s_{u,1}$ = 2, λ = 0.08, and ψ = 0.53; and (4) $s_{c,0}$ = 2, $s_{c,1}$ = 2, $s_{u,0}$ = 3, $s_{u,1}$ = 3, λ = 0.12, and ψ = 0.64. (F) X-ray diffraction analysis of selected magnetic extracts from different depths. Values shown on the right indicate the depth in core and diagrams at the bottom represent the powder X-ray diffraction peaks of the three minerals.

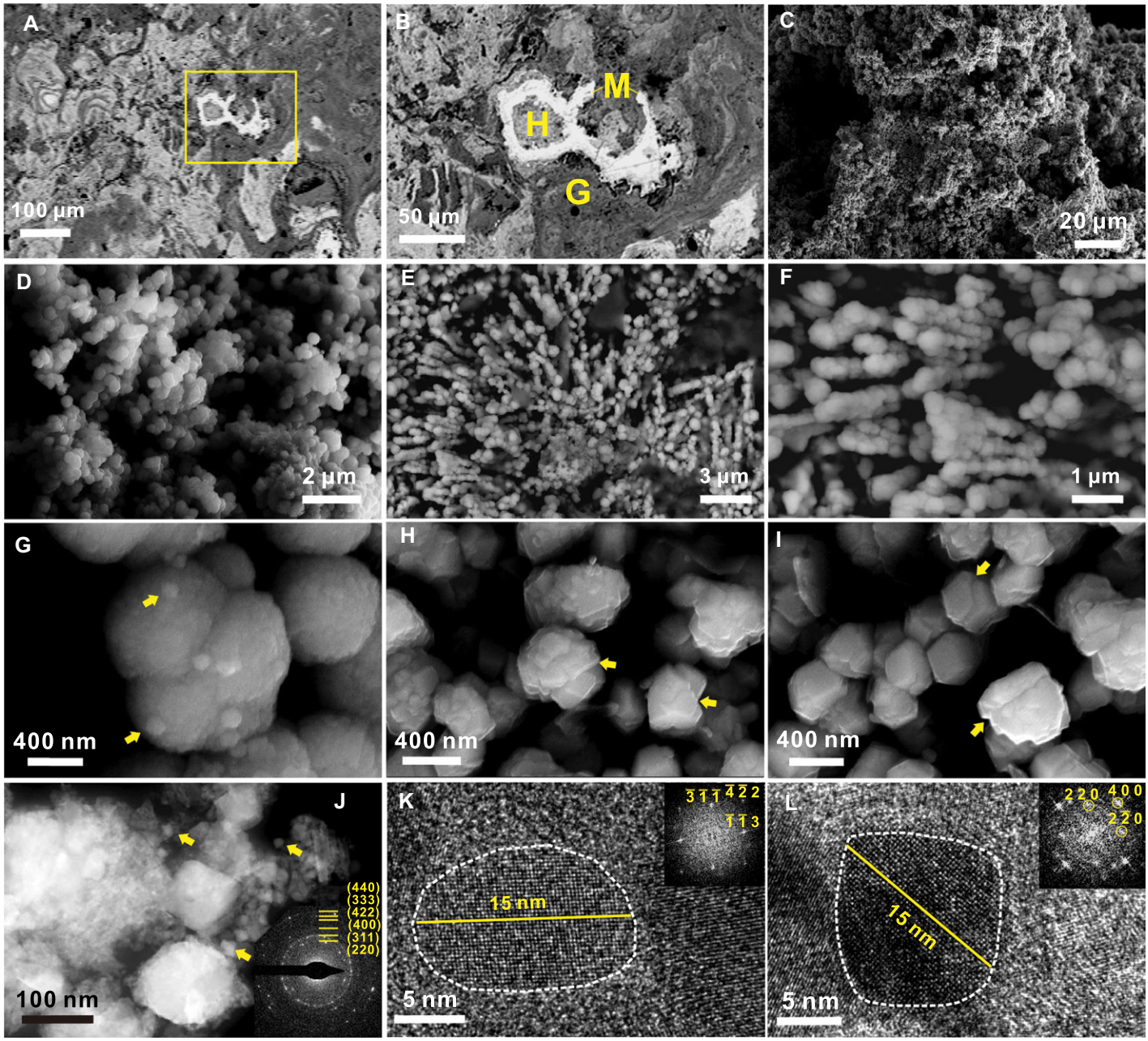

Figure 3. Morphologies and structure of magnetite particles in core GMGS2-16 in the South China Sea. (A,B) Polished thin section that reveals a paragenetic sequence of magnetite (M), goethite (G), and hematite (H) (backscattered electron images). Yellow rectangle in A is the area of B. (C,D) Aggregates of magnetite particles (scanning electron microscopy [SEM] images). (E,F) Magnetite particle alignments (SEM images). (G) Spherical particles (SEM images). Yellow arrows indicate smaller crystals. (H,I) Clustered euhedral crystals (SEM images). Yellow arrows indicate twin boundaries. (J) Aggregates of magnetite particles with various sizes (scanning transmission electron microscope [STEM] image). Yellow arrows indicate small single crystals, and inset is selected area electron diffraction pattern. (K,L) Lattice fringes for individual single magnetite crystals in high-resolution TEM images.

diagenetic sulfidization and magnetite dissolution (Roberts et al., 2018). In contrast, similar FORC diagrams were produced for samples with peak χ values (Figs. 2E2–2E4; Fig. S2D), which indicate the presence of stable SD particles with strong magnetostatic interactions and/or vortex-state particles (see Roberts et al. [2017] for signatures of vortex-state particles). Equidimensional SD magnetite has sizes in the ~20–75 nm range, and vortex-state particles have sizes in the hundreds of nanometers range (Muxworthy and Williams, 2009).

X-ray diffraction (XRD) analysis reveals that magnetite is the sole magnetic phase in the magnetic mineral extracts (Fig. 2F). This was confirmed by observations of clustered ultrafine particles within the magnetite aggregates, which range mainly from 200 to 800 nm in size (Fig. 3; Fig. DR3). Rarely, aligned magnetite particles were found (Figs. 3E and 3F; Figs. S3F–S3H), which differ from magnetofossil chains and are more similar to microbially formed structures (e.g., Johannessen et al., 2020). Individual particles are mainly spherical (Fig. 3G) or clustered euhedral crystals (Figs. 3H and 3I). Both particle types also occur as smaller nanocrystals (Figs. 3G–3I) with single-crystal sizes ranging from 10 to 20 nm (Figs. 3J–3L).

NATURE OF THE MAGNETITE NANOPARTICLES

Magnetite in marine sediments generally originates from detrital inputs from land or as an authigenic mineral that forms during diagenesis (Roberts, 2015). The ultrafine, well-crystallized, and aggregated nature of the studied particles

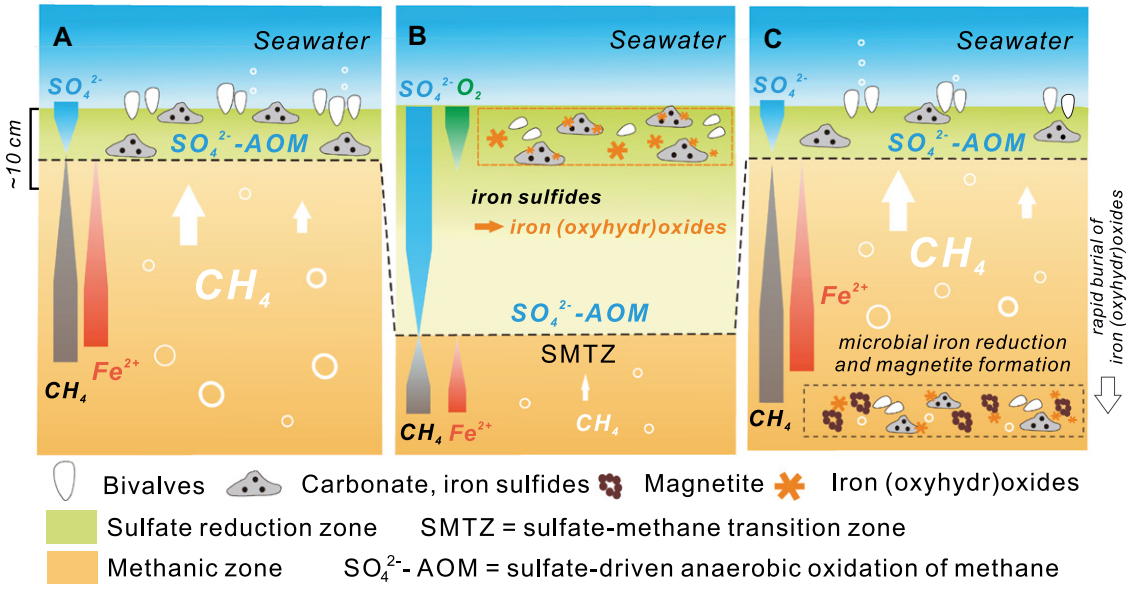

Figure 4. Simplified scenario for how magnetite precipitates in methanic sediments under the influence of variable seepage intensities. (A) During high seepage activity, the sulfate-methane transition zone (SMTZ) is located near the sediment surface where chemosymbiotic fauna occur. Within the SMTZ, sulfate-driven anaerobic oxidation of methane results in carbonate and iron-sulfide mineral precipitation. (B) After decline in seepage activity, downward-moving oxidizing fluids promote iron-sulfide mineral oxidation at the former SMTZ, which leads to secondary iron (oxyhydr)oxide formation. (C) When secondary iron (oxyhydr)oxides are exposed to methanic environments (see text for details), microbial iron reduction leads to authigenic magnetite formation. White circles indicate methane seepage flow.

(Fig. 3) excludes a detrital origin and indicates that the magnetite nanoparticles formed authigenically within the sediment, through either biologically mediated or inorganic mechanisms. Magnetofossils are a common source of ultrafine magnetite in sediment, which occur as single crystals with perfect morphology (Kopp and Kirschvink, 2008). The clustered structures of the studied magnetite particles, including crystal twinning (Figs. 3H and 3I), exclude an origin as intracellular magnetite produced by MTB. In contrast, extracellular magnetite produced by DIRB has irregular shapes without high structural perfection and normally ranges in size from 10 to 50 nm (Li et al., 2009). Most of our identified particles are much larger (as large as 800 nm in diameter), which makes them distinct from the reported characteristics of extracellular magnetite produced by DIRB. Thus, the nanoparticles appear to represent a new type of marine sedimentary magnetite.

Carbonate nodules strongly depleted in ^{13}C are distributed throughout core GMGS2-16 (Fig. 2C), and pyrite aggregates occur commonly in the carbonate-bearing layers (Lin et al., 2018). These observations indicate the former presence of locally pronounced sulfate-driven anaerobic oxidation of methane (cf. Jørgensen et al., 2004), likely coinciding with paleo-SMTZs (cf. Lin et al., 2018). Also, molybdenum and uranium enrichments in carbonate nodules (Chen et al., 2016), co-occurrence of bivalve shells, and low $\delta^{34}S$ in pyrite (Lin et al., 2018) indicate that the carbonate formed close to the seawater-sediment interface in association with high methane flux (cf. Chen et al., 2016; Lin et al., 2018). Most of the identified authigenic magnetite accumulated in such sulfide mineral–rich carbonate-bearing layers. This is unusual because magnetite is expected to be reduced in sulfidic environments (Riedinger et al., 2005; Roberts, 2015); the unprotected magnetite nanoparticles would be particularly unstable (Li et al., 2009) due to their high surface area and reactivity to hydrogen sulfide (Roberts, 2015). Abundant euhedral magnetite in such a sulfidic environment is puzzling and indicates that magnetite formation postdated most of the carbonate and pyrite formation at paleo-SMTZs, after the environment became hydrogen sulfide limited.

We propose the following scenario for magnetite authigenesis driven by microbial iron reduction within methanic sediments that undergo dynamic methane seepage changes (Fig. 4). Vertical SMTZ movement and variable redox conditions occur commonly in this gas hydrate–bearing area (Z. Lin et al., 2016). In initial stages with high methane fluxes, sulfide production would cause pyrite accumulation at a shallow SMTZ. When seepage diminishes, downward-moving, seawater-derived oxidizing fluids would promote iron-sulfide mineral oxidation at the former SMTZ, leading to secondary iron (oxyhydr)oxide (Fig. 3B; Fig. S1) and gypsum formation (Q. Lin et al., 2016). High porosity and permeability in coarse sediments (Chen et al., 2016) and advective seawater transport due to convective fluxes at seeps (Aloisi et al., 2004) would facilitate sulfide mineral oxidation. An ensuing change from oxic to methanic environments would then have been caused by a resurgence of high methane fluxes (Lin et al., 2018). Rapid sediment burial (e.g., mass wasting; Wang et al., 2016) would also promote iron (oxyhydr)oxide preservation during burial into a methanic environment. The presence of wüstite (FeO; Fig. 2F) suggests a sulfide-free Fe^{2+}-rich environment (cf. Kolo et al., 2009) and also indicates rapid burial of reactive iron (oxyhydr)oxides without further alteration by sulfidization.

Magnetite authigenesis has not been identified previously in methanic sediments, although microbial iron reduction is observed commonly in similar sedimentary settings (Egger et al., 2014; Riedinger et al., 2014; Amiel et al., 2020). Microbial iron reduction in methanic zones can be driven by (1) DIRB outcompeting methanogens for organic substrates (Thamdrup, 2000), (2) methanogens that switch from methanogenesis to iron reduction with an unidentified electron donor that does not appear to be methane (Sivan et al., 2016), or (3) iron reduction coupled to anaerobic oxidation of methane (Beal et al., 2009; Egger et al., 2014). Extracellular titanomagnetite has been identified under nearly natural methanic conditions in culture with the archaeon *Methanosarcina barkeri* (Shang et al., 2020). Based on this observation, microbially driven magnetite authigenesis with iron (oxyhydr)oxides as an electron acceptor (Fig. 3B; Fig. S1) could be feasible in methanic sediments. Organic substrates for dissimilatory iron reduction are probably scarce when these sediments are subjected to methanic conditions, which suggests that coupling of iron reduction to anaerobic oxidation of methane is the most likely process. Although the nature of iron reduction in methanic sediments is not clear, the presence of both microorganisms with iron reducing abilities and reactive Fe^{3+}-bearing minerals is essential for the process to occur. Methanogenic and/or methanotrophic archaea are present throughout the studied core (Cui et al., 2019). The presence of iron (oxyhydr)oxides in methanic sediments at site GMGS2-16 would, thus, allow authigenic magnetite formation by microbial iron reduction. Irrespective of the lack of laboratory culture studies of magnetite formation mechanisms in methanic sediments, the proposed scenario provides an explanation for why magnetite

accumulates alongside wüstite within methanic zones at levels coincident with paleo-SMTZs.

Studies of magnetism in methanic sediments have typically focused on magnetic-iron-sulfide authigenesis and magnetic-iron-oxide dissolution, which mainly result from sulfide release during sulfate-driven anaerobic oxidation of methane (Roberts, 2015). Ubiquitous magnetite dissolution in sulfidic environments (Roberts, 2015) means that methanic environments are generally extremely weakly magnetized unless magnetic iron sulfides form, and magnetite authigenesis is unexpected. As the first report of authigenic magnetite formation at a methane seep, we document a new source of marine sedimentary magnetization. Magnetite formation linked to microbial iron reduction within methanic sediments in dynamic seep environments allows the newly formed magnetite to escape sulfidic dissolution, which removes magnetite in shallow organic-rich sediments and benefits its longer-term preservation. Moreover, the discovered magnetite particles fall within a broad size range that spans the stable-SD to vortex magnetic domain states (Muxworthy and Williams, 2009), with the coarser end of the identified size range falling within the less magnetically stable multi-vortex to multi-domain size range (Roberts et al., 2017). The significant authigenic magnetite concentration in the stable-SD-state to single-vortex-state size range, which can carry stable long-term magnetization, could be an important source of sedimentary magnetic signals in marine sediments, although the recorded magnetization would be acquired with a post-depositional delay with respect to surrounding sediments. A deeper explanation of the magnetite formation process is hampered by incomplete understanding of microbial iron reduction in methanic environments and the unsteady nature of methane seepage. Future work is needed to resolve the mechanism(s) by which microorganisms generate magnetite in methanic environments. Our finding of a new type of authigenic marine sedimentary magnetite, with particle alignments resembling microbially formed structures in environments that favor coupling of iron reduction to anaerobic oxidation of methane, provides critical constraints for such work.

ACKNOWLEDGMENTS

This research was funded by the National Key Research and Development Program of China (grant 2018YFC0310004 and 2018YFA0702605), the National Natural Science Foundation of China (grants 41806049, 41876038, and 91128101), the Guangdong Special Fund for Economic Development (Marine Economy, grant GDME-2018D001), the China Geological Survey Project for South China Sea Gas Hydrate Resource Exploration (grant DD20160211), and the Australian Research Council (grant DP200100765). Zhiyong Lin acknowledges the International Postdoctoral Exchange Fellowship Program provided by the China Postdoctoral Council (20180053). We thank Shengxiong Yang and Guangxue Zhang for providing samples. Comments by Max Coleman, Ramon Egli, and an anonymous reviewer helped to improve the paper.

REFERENCES CITED

Aloisi, G., Wallmann, K., Haese, R.R., and Saliège, J.-F., 2004, Chemical, biological and hydrological controls on the ^{14}C content of cold seep carbonate crusts: Numerical modeling and implications for convection at cold seeps: Chemical Geology, v. 213, p. 359–383, https://doi.org/10.1016/j.chemgeo.2004.07.008.

Amiel, N., Shaar, R., and Sivan, O., 2020, The effect of early diagenesis in methanic sediments on sedimentary magnetic properties: Case study from the SE Mediterranean continental shelf: Frontiers of Earth Science, v. 8, 283, https://doi.org/10.3389/feart.2020.00283.

Beal, E.J., House, C.H., and Orphan, V.J., 2009, Manganese- and iron-dependent marine methane oxidation: Science, v. 325, p. 184–187, https://doi.org/10.1126/science.1169984.

Boetius, A., Ravenschlag, K., Schubert, C.J., Rickert, D., Widdel, F., Gieseke, A., Amann, R., Jørgensen, B.B., Witte, U., and Pfannkuche, O., 2000, A marine microbial consortium apparently mediating anaerobic oxidation of methane: Nature, v. 407, p. 623–626, https://doi.org/10.1038/35036572.

Chang, S.B.R., and Kirschvink, J.L., 1989, Magnetofossils, the magnetization of sediments, and the evolution of magnetite biomineralization: Annual Review of Earth and Planetary Sciences, v. 17, p. 169–195, https://doi.org/10.1146/annurev.ea.17.050189.001125.

Chen, F., Hu, Y., Feng, D., Zhang, X., Cheng, S., Cao, J., Lu, H., and Chen, D., 2016, Evidence of intense methane seepages from molybdenum enrichments in gas hydrate-bearing sediments of the northern South China Sea: Chemical Geology, v. 443, p. 173–181, https://doi.org/10.1016/j.chemgeo.2016.09.029.

Cui, H., Su, X., Chen, F., Holland, M., Yang, S., Liang, J., Su, P., Dong, H., and Hou, W.G., 2019, Microbial diversity of two cold seep systems in gas hydrate-bearing sediments in the South China Sea: Marine Environmental Research, v. 144, p. 230–239, https://doi.org/10.1016/j.marenvres.2019.01.009.

Devouard, B., Posfai, M., Hua, X., Bazylinski, D.A., Frankel, R.B., and Buseck, P.R., 1998, Magnetite from magnetotactic bacteria: Size distributions and twinning: American Mineralogist, v. 83, p. 1387–1398, https://doi.org/10.2138/am-1998-11-1228.

Egger, M., et al., 2014, Iron-mediated anaerobic oxidation of methane in brackish coastal sediments: Environmental Science & Technology, v. 49, p. 277–283, https://doi.org/10.1021/es503663z.

Egli, R., 2013, VARIFORC: An optimized protocol for calculating non-regular first-order reversal curve (FORC) diagrams: Global and Planetary Change, v. 110, p. 302–320, https://doi.org/10.1016/j.gloplacha.2013.08.003.

Heslop, D., Roberts, A.P., Oda, H., Zhao, X., Harrison, R.J., Muxworthy, A.R., Hu, P.-X., and Sato, T., 2020, An automatic model selection-based machine learning framework to estimate FORC distributions: Journal of Geophysical Research: Solid Earth: v. 125, p. e2020JB020418, https://doi.org/10.1029/2020JB020418.

Johannessen, K.C., McLoughlin, N., Vullum, P.E., and Thorseth, I.H., 2020, On the biogenicity of Fe-oxyhydroxide filaments in silicified low-temperature hydrothermal deposits: Implications for the identification of Fe-oxidizing bacteria in the rock record: Geobiology, v. 18, p. 31–53, https://doi.org/10.1111/gbi.12363.

Jørgensen, B.B., 1982, Mineralization of organic matter in the sea bed—The role of sulphate reduction: Nature, v. 296, p. 643–645, https://doi.org/10.1038/296643a0.

Jørgensen, B.B., Böttcher, M.E., Lüschen, H., Neretin, L.N., and Volkov, I.I., 2004, Anaerobic methane oxidation and a deep H_2S sink generate isotopically heavy sulfides in Black Sea sediments: Geochimica et Cosmochimica Acta, v. 68, p. 2095–2118, https://doi.org/10.1016/j.gca.2003.07.017.

Kolo, K., Konhauser, K., Krumbein, W.E., Van Ingelgem, Y., Hubin, A., and Claeys, P., 2009, Microbial dissolution of hematite and associated cellular fossilization by reduced iron phases: A study of ancient microbe-mineral surface interactions: Astrobiology, v. 9, p. 777–796, https://doi.org/10.1089/ast.2008.0263.

Kopp, R.E., and Kirschvink, J.L., 2008, The identification and biogeochemical interpretation of fossil magnetotactic bacteria: Earth-Science Reviews, v. 86, p. 42–61, https://doi.org/10.1016/j.earscirev.2007.08.001.

Li, Y.L., Pfiffner, S.M., Dyar, M.D., Vali, H., Konhauser, K., Cole, D.R., Rondinone, A.J., and Phelps, T.J., 2009, Degeneration of biogenic superparamagnetic magnetite: Geobiology, v. 7, p. 25–34, https://doi.org/10.1111/j.1472-4669.2008.00186.x.

Lin, Q., Wang, J., Algeo, T.J., Su, P., and Hu, G., 2016, Formation mechanism of authigenic gypsum in marine methane hydrate settings: Evidence from the northern South China Sea: Deep-Sea Research: Part I, Oceanographic Research Papers, v. 115, p. 210–220, https://doi.org/10.1016/j.dsr.2016.06.010.

Lin, Z., Sun, X., Lu, Y., Xu, L., Gong, J., Lu, H., Teichert, B.M.A., and Peckmann, J., 2016, Stable isotope patterns of coexisting pyrite and gypsum indicating variable methane flow at a seep site of the Shenhu area, South China Sea: Journal of Asian Earth Sciences, v. 123, p. 213–223, https://doi.org/10.1016/j.jseaes.2016.04.007.

Lin, Z., et al., 2018, Multiple sulfur isotopic evidence for the origin of elemental sulfur in an iron-dominated gas hydrate-bearing sedimentary environment: Marine Geology, v. 403, p. 271–284, https://doi.org/10.1016/j.margeo.2018.06.010.

Lovley, D.R., Stolz, J.F., Nord, G.L., and Phillips, E.J., 1987, Anaerobic production of magnetite by a dissimilatory iron-reducing microorganism: Nature, v. 330, p. 252–254, https://doi.org/10.1038/330252a0.

McDonnell, S.L., Max, M.D., Cherkis, N.Z., and Czarnecki, M.F., 2000, Tectono-sedimentary controls on the likelihood of gas hydrate occurrence near Taiwan: Marine and Petroleum Geology, v. 17, p. 929–936, https://doi.org/10.1016/S0264-8172(00)00023-4.

Moskowitz, B.M., 1995, Biomineralization of magnetic minerals: Reviews of Geophysics, v. 33, p. 123–128, https://doi.org/10.1029/95RG00443.

Moskowitz, B.M., Frankel, R.B., and Bazylinski, D.A., 1993, Rock magnetic criteria for the detection of biogenic magnetite: Earth and Planetary Science Letters, v. 120, p. 283–300, https://doi.org/10.1016/0012-821X(93)90245-5.

Muxworthy, A.R., and Williams, W., 2009, Critical superparamagnetic/single-domain grain sizes in interacting magnetite particles: Implications for magnetosome crystals: Journal of the Royal Society: Interface, v. 6, p. 1207–1212, https://doi.org/10.1098/rsif.2008.0462.

Pike, C.R., Roberts, A.P., and Verosub, K.L., 1999, Characterizing interactions in fine magnetic

particle systems using first order reversal curves: Journal of Applied Physics, v. 85, p. 6660–6667, https://doi.org/10.1063/1.370176.

Riedinger, N., Pfeifer, K., Kasten, S., Garming, J.F.L., Vogt, C., and Hensen, C., 2005, Diagenetic alteration of magnetic signals by anaerobic oxidation of methane related to a change in sedimentation rate: Geochimica et Cosmochimica Acta, v. 69, p. 4117–4126, https://doi.org/10.1016/j.gca.2005.02.004.

Riedinger, N., Formolo, M.J., Lyons, T.W., Henkel, S., Beck, A., and Kasten, S., 2014, An inorganic geochemical argument for coupled anaerobic oxidation of methane and iron reduction in marine sediments: Geobiology, v. 12, p. 172–181, https://doi.org/10.1111/gbi.12077.

Roberts, A.P., 2015, Magnetic mineral diagenesis: Earth-Science Reviews, v. 151, p. 1–47, https://doi.org/10.1016/j.earscirev.2015.09.010.

Roberts, A.P., Chang, L., Heslop, D., Florindo, F., and Larrasoaña, J.C., 2012, Searching for single domain magnetite in the "pseudo-single-domain" sedimentary haystack: Implications of biogenic magnetite preservation for sediment magnetism and relative paleointensity determinations: Journal of Geophysical Research, v. 117, B08104, https://doi.org/10.1029/2012JB009412.

Roberts, A.P., Almeida, T.P., Church, N.S., Harrison, R.J., Heslop, D., Li, Y., Li, J., Muxworthy, A.R., Williams, W., and Zhao, X., 2017, Resolving the origin of pseudo-single domain magnetic behavior: Journal of Geophysical Research: Solid Earth, v. 122, p. 9534–9558, https://doi.org/10.1002/2017JB014860.

Roberts, A.P., Zhao, X., Harrison, R.J., Heslop, D., Muxworthy, A.R., Rowan, C.J., Larrasoaña, J.C., and Florindo, F., 2018, Signatures of reductive magnetic mineral diagenesis from unmixing of first-order reversal curves: Journal of Geophysical Research: Solid Earth, v. 123, p. 4500–4522, https://doi.org/10.1029/2018JB015706.

Sha, Z., Liang, J., Zhang, G., Yang, S., Lu, J., Zhang, Z., McConnell, D.R., and Humphrey, G., 2015, A seepage gas hydrate system in northern South China Sea: Seismic and well log interpretations: Marine Geology, v. 366, p. 69–78, https://doi.org/10.1016/j.margeo.2015.04.006.

Sha, Z., Xu, Z., Fu, S., Liang, J., Zhang, W., Su, P., Lu, H., and Lu, J., 2019, Gas sources and its implications for hydrate accumulation in the eastern Pearl River Mouth Basin: Haiyang Dizhi Yu Disiji Dizhi (Marine Geology and Quaternary Geology), v. 39, p. 116–125, https://doi.org/10.16562/j.cnki.0256-1492.2019010902 (in Chinese with English abstract).

Shang, H., Daye, M., Sivan, O., Borlina, C.S., Tamura, N., Weiss, B.P., and Bosak, T., 2020, Formation of zero-valent iron in iron-reducing cultures of *Methanosarcina barkeri*: Environmental Science & Technology, v. 54, p. 7354–7365, https://doi.org/10.1021/acs.est.0c 01595.

Sivan, O., Shusta, S.S., and Valentine, D.L., 2016, Methanogens rapidly transition from methane production to iron reduction: Geobiology, v. 14, p. 190–203, https://doi.org/10.1111/gbi.12172.

Thamdrup, B., 2000, Bacterial manganese and iron reduction in aquatic sediments: Advances in Microbial Ecology, v. 16, p. 41–84, https://doi.org/10.1007/978-1-4615-4187-5_2.

Wang, L., Yu, X., Tyson, S., Li, S., Kuang, Z., Sha, Z., Liang, J., and He, Y., 2016, Submarine landslides, relationship with BSRs in the Dongsha area of South China Sea: Petroleum Research, v. 1, p. 59–69, https://doi.org/10.1016/S2096-2495(17)30031-5.

Printed in USA